ACS APPLIED MATERIALS & INTERFACES

Energy, Environmental, and Catalysis Applications

Understanding the thermal treatment effect of two dimensional siloxene sheets and the origin of superior electrochemical energy storage performances

Parthiban Pazhamalai, Karthikeyan Krishnamoorthy, Surjit Sahoo, Vimal Kumar Mariappan, and Sang-Jae Kim

ACS Appl. Mater. Interfaces, **Just Accepted Manuscript** • DOI: 10.1021/acsami.8b15323 • Publication Date (Web): 26 Nov 2018

Just Accepted

ACS Publications

is published by the American Chemical Society. 1155 Sixteenth Street N.W., Washington, DC 20036

Understanding the thermal treatment effect of two dimensional siloxene sheets and the origin of superior electrochemical energy storage performances

Parthiban Pazhamalai[1#], Karthikeyan Krishnamoorthy[2#], Surjit Sahoo[1],

Vimal Kumar Mariappan[1], Sang -Jae Kim[1, 3*]

[1]Department of Mechatronics Engineering, Jeju National University, Jeju 63243, South Korea.

[2]Nanomaterials laboratory, Department of Mechanical Engineering, Jeju National University, Jeju 63243, South Korea.

[3]Department of Advanced Convergence Science & Technology, Jeju National University, Jeju 63243, South Korea.

[#] These authors contributed equally to this work.

Corresponding author Email: kimsangj@jejunu.ac.kr

ABSTRACT:

Two dimensional siloxene sheets are an emerging class of materials with eclectic range of potential applications including electrochemical energy conversion and storage sectors. Here we have demonstrated the dehydrogenation/dehydroxylation of siloxene sheets by thermal annealing at high temperature (HT) and investigated their supercapacitive performances using ionic liquid electrolyte. The X-ray diffraction analysis, spectroscopic (FT-IR, laser Raman, and XPS) studies and morphological analysis of HT-siloxene revealed the removal of functional groups at the edges/basal planes of siloxene, and preservation of oxygen interconnected Si_6 rings with sheet-like structures. The HT-siloxene symmetric supercapacitor (SSC) operates over a wide potential window (0 to 3.0 V), delivers a high specific capacitance (3.45 mF cm^{-2}), high energy density of about 15.53 mJ cm^{-2} (almost two-fold higher than as-prepared siloxene SSC), low equivalent series resistance (compared to reported silicon based SSCs) with excellent rate capability and long cycle life over 10,000 cycles.

KEYWORDS: Siloxene; Thermal treatment; 2D material; Supercapacitors; Energy Density; Electrochemical Impedance Spectroscopy.

1. Introduction

The advent of two dimensional materials beyond graphene created new horizons on the development of next-generation energy storage devices[1]. Two dimensional materials such as transition metal dichalcogenides[2], transition metal carbides/nitrides/carbonitrides[3,4], metal organic frameworks[5], and polymers[6] are developed and examined for application as advanced electrode materials for flexible and wearable energy storage devices (batteries and supercapacitors) during this era. Several research works have been focused on development of novel electrode materials and their utilization towards different types of supercapacitors such as (i) aqueous supercapacitors[7], (ii) hybrid ion supercapacitors[8], (iii) colloidal supercapacitors[9], and (iv) non-aqueous supercapacitors[10], respectively. Recent studies demonstrated the possibility of utilizing 2D metals such as boron, germanium, phosphorus as an electrode for supercapacitor devices as an alternative to graphene[11–13]. However, the development of silicon-based materials for high performance supercapacitors are beneficial for ease of integration with the existing silicon technology in the semiconductor industry[14]. Thus, plentiful research is ongoing on the energy storage properties of various silicon materials such as silicon wires, rods, flowers, and sheets, etc[15–18]. In this scenario, silicene, a 2D allotrope of silicon (with sp^3 hybridization) received increasing attention owing to their unique structural and electrical properties[19–21]. Theoretical studies suggested the high possibilities of silicene in various fields including an electronic device, spintronics, ferromagnetism, optoelectronics, sensors, hydrogen storage, catalysis, water splitting, and oxygen reduction reaction, as well as novel electrodes for electrochemical energy storage devices[22–24]. However, experimental findings for many of the above-mentioned theoretical predictions are not yet demonstrated. This is due to the lack of appropriate methods for the preparation of high-quality silicene in bulk scale[19]. High-quality silicene sheets can be grown on the surface of suitable

substrates (silver, iridium, MoS_2) via molecular beam epitaxy method whereas the lateral size of the as-grown silicene is in the range of very few nanometers, thus limits the research on silicene towards functional applications[25,26]. Hitherto, alternative routes are developed recently to obtained silicene-like materials using chemical and electrochemical methods.

Various chemical methods available for the preparation of silicene-like materials are reported viz (i) topotactic transformation of layered calcium silicide in presence of hydrochloric acid results in the formation of siloxene sheets (oxygen functionalized silicene)[27], (ii) iodine mediated liquid oxidation and exfoliation of $CaSi_2$ resulting in the formation of silicene sheets[28], (iii) magnesiothermic reduction of SiO_2 at elevated temperatures resulting in the formation of silicene flowers[29], (iv), electrochemical lithiation and de-lithiation of silicon which resulting in the formation of oxidized silicenes, respectively[30]. All these methods resulted in the formation of silicene sheets functionalized with oxygen in which the oxygen content varies in accordance with the preparation methods employed (such as reaction precursors, reaction temperature, and environment)[27–30]. The silicene-like materials reported being a promising anode material for Li-ion batteries as well as an electrode for high performance supercapacitor devices[31,32]. Our recent work demonstrated that the chemically prepared siloxene sheets as high-performance electrode materials for supercapacitors with a high energy density of 9.82 mJ cm^{-2} (higher compared to the reported silicon-based SCs)[33]. The siloxene sheets with oxidized functional groups on the surfaces of 2D silicon can be considered as analogs to graphene oxides (oxidized graphene, a well know precursor for preparation of chemically derived graphene's). Based on the different structures of siloxene, it can be classified into three major types (i) Weiss siloxene, (ii) chain-like siloxene and (iii) Kautsky-type siloxene[34]. It is expected that the removal of oxidized functional groups in the siloxene sheets can lead to reduced siloxene sheets which might possess higher electronic

conductivity. Until now, there are no such studies has been attempted to investigate the chemical structure of reduced siloxene sheets and their electrochemical properties. Thus, understanding the effect of high-temperature heat treatment (HT) process on the siloxene sheets might provide new insights such as (i) tailoring the functional groups, (ii) preservation of sheet-like structures or not, and (iii) lead to the possible routes for achieving chemically derived silicene or reduced siloxene sheets. Further, the reduced siloxene sheets with improved electronic conductivity (than siloxene sheets) can make them as an ideal candidate for supercapacitor. Therefore, in this work, we aimed to the remove the oxygenated groups from the siloxene sheets via a high-temperature treatment and investigated their chemical nature as well as applications in SCs.

2. Experimental section

2.1 Materials and methods

Calcium silicide ($CaSi_2$), and polyvinylidene fluoride (PVDF) were purchased from Sigma Aldrich Ltd., South Korea. 1-Ethyl-3-methylimidazolium tetrafluoroborate ($EMIMBF_4$) were purchased from Alfa Aesar Chemicals, South Korea. Hydrochloric acid (HCl), carbon black, and N-Methyl-2-pyrrolidone (NMP) were obtained from Dae-Jung Chemicals Ltd, South Korea. Ultrasound irradiation was carried out in a VCX 750 ultrasonicator (Sonics and Materials, Inc, USA, (20 kHz, 750 W)) using a direct-immersion titanium horn.

2.2 Topochemical transformation of $CaSi_2$ into siloxene sheets

In a typical synthesis method, 2D siloxene sheets was prepared via topochemical transformation of calcium silicide in an ice-cold hydrochloric acid[33]. Briefly, to synthesize siloxene sheets, $CaSi_2$ powders (1 g) were stirred in concentrated HCl (100 mL) at 0 °C for 4 days. The transformation from black color to green color confirms the dissolution of calcium in the HCl solution. Upon completion of the reaction, the obtained green colored siloxene sheets was washed

with acetone and water. The washed powder was dispersed in water (100 mL) and subjected to ultrasound irradiation for 1 h. Again, the siloxene sheets were washed with water and allowed to dry at 80 °C for 12 h. The as prepared siloxene sheets were denoted as p-siloxene.

2.3 Thermal annealing of siloxene sheets

Briefly, 1 g of as prepared siloxene sheets was well grounded and annealed at 200 °C for 2 h at a heating rate of 2 °C; and then the temperature was ramped to 900 °C at a heating rate of 10 °C, was kept for 6 h in an Ar atmosphere for the removal of functional groups attached at the edges of the siloxene sheets, followed by cooling to room temperature. A white greyish powder was formed as a result thermal annealing. The obtained heat treated siloxene powder was collected and used for further characterization. The siloxene sheets prepared via heat treatment were denoted as HT-siloxene sheets.

2.4 Instrumentation

X-ray diffraction pattern of the siloxene and HT-siloxene was collected using X-Ray Diffractometer System (X'pert pro MPD) with Cu-Kαradiation (λ=1.5418Å) (KBSI, Daegu Center). The functional groups in siloxene and HT-siloxene were examined using FT-IR spectroscopy (Thermo Scientific FT-IR spectrometer (Nicolet 6700)). Raman spectra were obtained using a LabRam HR Evolution Raman spectrometer (Horiba Jobin-Yvon, France). The chemical state of elements in the siloxene and HT-siloxene was analyzed using X-ray photoelectron spectrometer (ESCA-2000, VG Microtech Ltd.) measured at Korea Basic Science Institute (KBSI), Busan centre. The surface morphology and elemental mapping analysis was examined using field-emission scanning electron microscopy (TESCAN, MIRA3) and high-resolution transmission electron microscopy (JEM-2011, JEOL) measured at Korea Basic Science Institute (KBSI), Busan centre. The surface area and pore size distribution were measured at 77 K

using a NOVA 2000 system (Quantachrome, USA). The atomic force microscopic analysis of HT-siloxene sheets was measured using Digital Instruments, Nanoscope V multimode 8 (KBSI, Jeonju Centre).

2.5 Preparation of electrodes

Initially, the homogeneous slurry of working electrode was prepared by grinding active material (90 wt %) with 5 wt % of carbon black and 5 wt % of PVDF binder dispersed in NMP. Then the prepared slurry was spread onto an aluminum(Al) foil using doctor blade to ensure the uniformity of the electrode thickness. The electrode was dried at 80 °C in a vacuum oven to evaporate the solvent. After complete drying of the electrode coated on Al, it is subjected to be densely pressed by a rolling press machine (WCRP-1015G), and the electroactive mass of the HT-siloxene electrode was calculated from the difference between the mass of the Al foil before and after coating using Dual-range Semi-micro Balance (AUW-220D, SHIMADZU) with an approximation of five-decimal points is approximate ~0.5 mg in each substrate. For the coin cell fabrication, the electrode was cut into a circle shape with a diameter of 14 mm.

2.6 Fabrication and testing of symmetric supercapacitor device

The symmetric supercapacitor (SSC) device based on p-siloxene and HT-siloxene (HT-siloxene) sheets was fabricated with a CR2032 coin cell configuration with electroactive area of 1.54 cm^2 separated by a Celgard membrane. $EMIMBF_4$ is used as the electrolyte. The fabricated SSC device was crimped using an electric coin cell crimping and disassembling machine (MTI, Korea). All the electrolyte handling and device fabrication were carried out in a glove box with less than 1 ppm of moisture and oxygen. Electrochemical characterization of the SSCs were analyzed using cyclic voltammetry (CV) at various scan rates, EIS analysis in the frequency range from 0.01 Hz to 100 kHz at an amplitude of 10 mV, and galvanostatic charge-discharge (CD)

measurements using different current ranges were performed using an Autolab PGSTAT302N electrochemical workstation. The methods used for determining specific capacitance, energy/power density, and maximal power density of HT-siloxene SSC device is provided with the electronic supporting document.

3. Results and discussion

Figure 1 shows the schematic representation of the preparation of reduced siloxene sheets via high-temperature treatment of siloxene sheets (prepared via topochemical reaction of layered calcium disilicide ($CaSi_2$)). A topochemical reaction between the layered $CaSi_2$ with ice-cold HCl results in the de-intercalation of Ca ions from $CaSi_2$ and simultaneous formation of siloxene sheets comprising various functional groups (oxygen interconnected with Si_6 rings, Si-OH, Si-H, and $OSi_2{\equiv}Si{-}H$ functionalized at the edges and basal planes) as shown in Figure 1(A and B)[27,33,35]. Upon thermal annealing at a temperature of 900 °C, some of the functional groups attached to the siloxene sheets (Figure 1 (C)) are decomposed and results in the structure given in Figure 1 (D). The color of the pristine siloxene sheets (green color) was changed into a grey colored (See Figure S1, SI) after the HT process which might be due to the removal of functional groups attached with the siloxene sheets. The siloxene sheets prepared via topochemical reaction and HT process were denoted as p-siloxene and HT-siloxene sheets, respectively.

Figure 2 represents the comparative physico-chemical characterization of the p-siloxene and the HT-siloxene sheets. Figure 2(A) shows the X-ray diffraction (XRD) pattern indicating the presence of two diffraction peaks in the p-siloxene sheets observed at 13.5° and 26° which corresponds to the (001) and (100) planes of bi-dimensional silicon sheets derived from layered calcium disilicide via a topochemical reaction[36]. After thermal treatment, significant changes have been observed in the XRD pattern of HT-siloxene sheets as follows: (i) the peak observed at 13.5°

(interlayer spacing of 0.65 nm) was diminished completely, and (ii) the broad peak observed at 26° (interlayer spacing of 0.33 nm) was preserved even after the high temperature treatment. This might be due to the removal of oxygenated functional groups at the edges and basal planes of p-siloxene under HT process[37–39]. This effect is similar to that of thermal reduction of graphene oxide into graphene sheets[39,40]. This suggested that the thermal treatment of p-siloxene sheets resulted in the removal of oxygenated functional groups and the 2D silicon backbone was preserved. This finding is in agreement with the study of Yamanaka et al[27]. The bonding nature of the functional groups present in the p-siloxene and HT-siloxene sheets were examined using Fourier transformed infrared (FT-IR) spectroscopy as shown in Figure 2(B). The FT-IR spectrum of p-siloxene sheets shows the presence of broad vibration bands observed at 452, 867, 1034, 1639, and 2140 cm^{-1} which correspond to the vibrations raised from the ν(Si–Si), ν(Si–H), ν(Si–O–Si), ν(Si–OH), and ν(OSi_2≡Si–H), respectively[41]. The FT-IR spectrum of p-siloxene treated at various temperatures from 300 to 900 °C is provided in Figure S2, SI. This study revealed that the dehydrogenation of Si-H groups was occurred at a temperature of 400 °C, whereas the removal of Si-OH and OSi_2≡Si-H groups were removed at a temperature of 600 °C. Hitherto, the intercalated hydroxyl groups (3100 – 3600 cm^{-1}) has been completely removed at a temperature of 900 °C. This finding is in agreement with the previous study of Yamanaka et al.[37] After the HT process at a temperature of 900 °C , the following changes occurred in the FT-IR spectrum of HT-siloxene as follows: (i) the vibration bands of ν(Si–OH), ν(OSi_2≡Si–H), and ν(Si–H) groups diminished completely suggesting their thermal decomposition at higher temperatures, (ii) The band correspond to ν(Si–O–Si) become broadened due to the thermal shock faced by the oxygen-enriched hexagonal silicon rings which leads to the formation of a new band observed at 805 which corresponds to the ν(Si–O), and (iii) the ν(Si–Si) band (at 452 cm^{-1}) becomes more sharpened after the HT-process.

The crystallinity and bonding nature of the p-siloxene and HT-siloxene sheets were examined using laser Raman spectroscopy as shown in Figure 2(C). The laser Raman spectrum of p-siloxene sheets shows the presences of two sharp bands two bands at 495 and 525 cm^{-1} attributed to the vibrations of Si–O/Si-OH and Si–Si bonds, respectively[33]. The presence of Si-H bonding (640 and 740 cm^{-1}) in the p-siloxene sheets is also evident from the Raman spectrum. After HT process, the only one sharp band at 516 cm^{-1} was observed in the Raman spectrum of HT-siloxene sheets which corresponds to the vibration raised from symmetric stretching (E_{2g}) modes of Si-Si bonds present in the hexagonal Si_6 rings; this confirms the integrity of the 2D bi-dimensional structure even after HT process. This finding is in close agreement with the previous study on the Raman spectrum of 2D silicon prepared via lithiation and de-lithiation process[30]. Typical X-ray photoelectron survey spectrum (Figure S3, SI) of p-siloxene and HT-siloxene sheets shows the presence of Si 2p and O 1s states of elements at binding energies 102 and 530 eV respectively. The core-level spectrum O 1s states (see Figure S4, SI) which arises due to the presence of oxygen in the interconnected Si rings of the HT-siloxene sheets. Figure 2(D) shows the core-level spectrum of Si 2p states in the p- siloxene sheets and HT-siloxene sheets which showed significant changes as follows: The core-level spectrum of Si 2p states in p-siloxene sheets can be resolved into two components (i) Si-Si bonding (eV) and Si-O bonding (eV), respectively. After the HT process, the Si-Si component disappeared, and only one peak at 101.5 eV (Si-O bonding) was observed in the Si 2p core-level spectrum of HT- siloxene sheets. The disappearance of Si-Si peak in the core-level spectrum of HT-siloxene is in agreement with the previous study on the XPS analysis of heat-treated Wohler siloxene sheets[38]. Figure 3(A-G) represents the high-resolution transmission electron microscopic (HR-TEM) images and elemental mapping spectrum of the HT-siloxene. The HR-TEM images revealed the presence of sheet-like morphologies with few layers, suggesting

that the HT process did not affect the 2D structure of p-siloxene. The atomic force micrograph (AFM) of the HT-siloxene sheets were provided in Figure 3(D) and the section analysis of various sheets were provided in Figure S5 and S6 (SI), respectively. Figure 3 (D) represents the presence of sheet-like morphologies of the HT-siloxene which agrees with the HR-TEM micrographs. The section analysis of the HT-siloxene sheets (Figure S5 and S6, SI) revealed that the thickness of the sheets is in the range of 0.5 to 0.8 nm suggesting the presence of monolayer and/or bilayers of HT-siloxene sheets[36]. The elemental mapping images of HT-siloxene sheet (Figure 3(E-H)) indicates the presence of Si atoms (red-colored) and O atoms (grey-colored) distributed throughout the sheets. The O/Si ratio of the HT-siloxene sheets was found to be 1.17 % determined using Cliff-Lorimer thin ratio section analysis (see Figure S7, SI). The O/Si ratio of HT-siloxene is lower compared to that of the p-siloxene sheets (1.49 %)[33] which confirms the decrease in oxygen content after HT-process. The field emission scanning electron microscopic (FE-SEM) images of the HT-siloxene sheets indicates the presences of sheet-like structures (see Figure S8(A-D), SI) and the elemental mapping analysis (see Figure S9(A-D), in SI) indicates the presence of Si and O atoms in the HT-siloxene sheets. Figure S10 (SI) represents the N_2 adsorption-desorption isotherms of the HT-siloxene sheets indicating the high surface area of about 64.2 m^2 g^{-1} (which is higher than that of the surface area of siloxene sheets (59.72 m^2 g^{-1})) with an average pore size in the range of 30 to 40 nm respectively. These physico-chemical characterizations of HT-siloxene sheets suggested the removal of oxygenated functional groups such as Si-OH and $OSi_2{\equiv}Si{-}H$ groups at the basal planes and edges of the p-siloxene sheets. The removal of these functional groups might provide distinct electrochemical performances of HT-siloxene sheets compared to the p-siloxene sheets.

The electrochemical energy storage performance of the HT-siloxene sheet as electrodes were characterized via the fabrication of coin-cell type symmetric supercapacitors (SSC) with 1-Ethyl-3-methylimidazolium tetrafluoroborate ($EMIMBF_4$) as electrolyte. Figure S11 (SI) shows the CV profiles of the HT-siloxene SSC measured using a scan rate of 100 mV s^{-1} with different OPWs (0 to 3.0 V) which indicates that the fabricated SSC can operate over a wide OPW of 3.0 V. Figure 4 (A) shows the comparative CV profiles of the p-siloxene and HT-siloxene sheets based SSCs in $EMIMBF_4$ electrolyte obtained at a scan rate of 100 mV s^{-1}. It shows the presence of quasi-rectangular CV profiles for both SSCs over the operating potential window (OPW) of about 3.0 V. The current range in the CV profiles is higher for the HT-siloxene SSC compared to p-siloxene SSC, thus indicating the superior electrochemical energy storage performance of the HT-siloxene SSC. The CV profiles of HT-siloxene SSC shows the presence of a small peak observed at a cell voltage of 0.3 V which indicates the conformation change of electrochemical ions inside the micropores of HT-siloxene electrodes during electrochemical charging/discharging cycle[42]. Figure 4(B and C) shows the CV profiles of the HT-siloxene SSC obtained under different scan rates ranging from 25 to 1000 mV s^{-1}, respectively. The increasing current values and the retained quasi-rectangular nature of the HT-siloxene SSC with an increase in scan rates, suggest the better electrochemical capacitive nature of the HT-siloxene electrodes. The CV profiles of the p-siloxene SSC recorded at different scan rates is also provided (see Figure S12, SI). The effect of scan rate on the specific capacitance of p-siloxene and HT-siloxene based SSCs are provided in Figure 4(D). A maximum areal specific capacitance of about 3.09 mF cm^{-2} (equivalent to gravimetric specific device capacitance of 4.76 F g^{-1}) was obtained for the HT-siloxene SSC which is almost 1.47-fold higher compared to the specific capacitance of p-siloxene SSC (2.10 mF cm^{-2} or 3.24 F g^{-1}) obtained using a scan rate of 25 mV s^{-1}. With an increase in scan rate upto ten-fold,

the HT-siloxene SSC retains a specific capacitance upto 91.6 % whereas the p-siloxene SSC retains only 40.45 %. Further, increase in scan rate upto 40-fold (1000 mV s^{-1}), the HT-siloxene SSC still retained a specific capacitance of about 83.54 % whereas the p-siloxene SSC retains only 23.68 %. These studies suggested the enhancement of specific capacitance in HT-siloxene based SSCs with superior rate capability compared to p-siloxene SSCs.

Figure 5(A) represents the comparative galvanostatic CD profile of p-siloxene and HT-siloxene SSCs recorded using a constant current of 0.25 mA, respectively. It evidences that the charging and discharging time of the HT-siloxene SSC is quite higher to that of the p-siloxene SSC, thus indicating superior energy storage properties of the HT-siloxene SSC. The CD profiles of HT-siloxene SSC recorded using different applied current ranges are shown in Figure 5(B) which displayed the presence of quasi-symmetric CD profiles, an indication of predominant charge-storage due to pseudocapacitive nature[43]. The CD profiles of the p-siloxene SSC recorded at different applied current ranges are also provided (see Figure S13, SI). The effect of applied current on the specific capacitance of HT-siloxene SSC is provided in Figure 5(C). The maximum specific capacitance of 3.45 mF cm^{-2} (equivalent to gravimetric specific device capacitance of 5.31 F g^{-1}) is obtained for the HT-siloxene SSC recorded at a current of 0.25 mA, which is 1.71 times higher than the p-siloxene SSC (specific capacitance of 2.02 mF cm^{-2} (equivalent to gravimetric specific capacitance of 3.11 F g^{-1}) and those of reported SSCs using silicon electrodes in organic electrolyte (See Table S1, SI). The rate capability, cyclic stability, energy and power density are some of the important features which determine the practical applications of a supercapacitor device[33,44]. Figure 5(D) shows the rate capability of the HT-siloxene SSC which showed better capacitance retention and stable cycling (over 50 cycles) with different applied current ranges from low to high and high to low. This study demonstrated the excellent rate performance of HT-

siloxene SSC. The energy/power performance metrics of the HT-siloxene SSC (in comparison with p-siloxene SSC and other silicon-based SSCs)) is presented in the form of Ragone plot (Figure 6 (A)). The HT-siloxene SSC possesses a high energy density of about 15.53 mJ cm^{-2} (equivalent to gravimetric energy density of 6.64 Wh Kg^{-1}) with a corresponding power density of 0.24 mW cm^{-2} (equivalent to gravimetric power density of 375 W kg^{-1}) as obtained from the CD profiles using a current range of 0.25 mA, respectively. At the same current range, the p-siloxene SSC possesses an energy density of about 9.09 mJ cm^{-2} or 3.89 Wh Kg^{-1} with a corresponding power density of 0.24 mW cm^{-2} or 375 W kg^{-1}. With an increase in current ranges upto 10 mA, the energy density of p-siloxene and HT-siloxene SSCs are found to be 2.14 and 9.05 mJ cm^{-2} (0.91 and 3.875 Wh kg^{-1}), whereas the power density increases upto 9.74 mW cm^{-2} (equivalent to gravimetric power density of 15000 W kg^{-1}), respectively. Thus, the removal of functional groups in the p-siloxene sheets via thermal treatment results in providing superior energy density without compensating the power density. Further, the Ragone plot also highlights the superior performance metrics of the HT-siloxene with other silicon-based SSCs as well. The energy density of the HT-siloxene SSC is quite higher compared to other SSCs such as silicon nanowires (190 μJ cm^{-2})[45] , diamond coated Si NWs (2.5 mJ cm^{-2})[46], PEDOT coated Si NW (9 mJ cm^{-2})[47], polypyrrole coated Si NW (11 mJ cm^{-2})[15] and polypyrrole coated Si NTr (15 mJ cm^{-2})[15], graphene/Si NW (3.6 mJ cm^{-2})[48] and diamond coated Si NW (11 mJ cm^{-2})[49].

The superior capacitive nature and charge-transfer kinetics of the HT-siloxene SSC over p-siloxene SSC was analyzed in detail using EIS measurements in the frequency range of 0.01 Hz to 100 KHz at an amplitude of 10 mV, and the results are presented in the form of Nyquist and Bode plots. Figure 6(B) shows the Nyquist plot (plot of real against the imaginary component of the impedance) of p-siloxene and HT-siloxene SSCs. The Nyquist plot of both SSCs revealed the

presence of three characteristic regions viz. (i) low-, (ii) intermediate- and (iii) high- frequency regions from which important parameters such as Warburg line, Knee frequency, and equivalent series resistance (ESR) of the devices[33,50]. At first, the low-frequency region shows the presence of Warburg line (an indication of diffusion controlled reaction) which is closer to the imaginary axis for the HT-siloxene SSC compared to that of the p-siloxene SSC, thus indicating the better capacitance of the former[51]. The knee frequency observed at the intermediate frequency region is about 10 and 100 Hz for the p-siloxene and HT-siloxene SSCs, respectively. The ESR of the p-siloxene and HT-siloxene SSCs can be determined from the low- frequency region (see inset of Figure 6(B)) which was found to be 3.86 and 2.34 Ω, respectively[52]. The low ESR of the HT-siloxene SSC might be attributed to the removal of oxidized functional groups from the p-siloxene. The ESR of the HT-siloxene SSC is quite lower compared to the reported ESR values of silicon-based SSCs (Si NWs (22 Ω)[45], diamond-coated Si NWs (7 Ω)[46], Si NTs (17 Ω)[53]). A low ESR can results in obtaining maximal power density of a supercapacitor (since $P_{max} = V^2/4ESR$)[44]. The low ESR of HT-siloxene SSC leads to a high maximal power density values of about 627.05 mW cm^{-2} compared to that of p-siloxene SSC (P_{max} = 429.46 mW cm^{-2}). The obtained maximal power density of HT-siloxene SSC is higher compared to the recent works of silicon-based SSCs (Si NWs (182 mW cm^{-2}) [45], diamond-coated Si NWs (321 mW cm^{-2})[46], Si NTs (235 mW cm^{-2})[53], and Si NWs of 20 μm (1.4 mW cm^{-2})[54]). The Bode phase angle plots of the p-siloxene and HT-siloxene SSCs are shown in Figure 6(C) which indicates the change in phase angle with respect to applied frequency. The phase angle at the low frequency region is often used to characterize the capacitive nature of the device[7]. The phase angle at the low frequency region (0.01 Hz) is found to be 71.85° and 83.38° for the p-siloxene and HT-siloxene SSCs demonstrating the better capacitive nature in the later. The capacitor response frequency (f_o) at the phase angle of -45° was 4.67 Hz for HT-

siloxene SSC much higher than that of p-siloxene SSC (0.9668 Hz). Thus, the corresponding time constant ($\tau_o=1/f_o$) was only 0.214 s for HT-siloxene SSC, compared to 1.034 s for p-siloxene SSC. The low time constant (time required to discharge all the energy with an efficiency of >50%) strongly suggest that the HT-siloxene SSC possess huge potential for instantaneous delivery of ultra-high power and energy. Table S2 (SI) summarizes the parameters derived from EIS spectrum of p-siloxene and HT-siloxene SSCs. Figure 6 (D) shows the capacitance retention of HT-siloxene SSC over 10,000 cycles recorded at a current range of 5 mA. A capacitance retention of 96.3 % of the initial capacitance was obtained for the HT-siloxene SSC, thus demonstrating their better electrochemical stability over prolonged cycles. Figure S14 (A-D), SI shows that the FE-SEM micrographs of HT-siloxene electrode before and after the electrochemical cyclic tests which demonstrated that there are no structural changes occurred at the HT-siloxene electrode even after 10,000 cycles of continuous CD measurements[55]. Further, the FE-SEM micrograph of HT-siloxene electrode after cyclic test revealed that the electroactive material is completely wetted with the electrolyte ions. The elemental mapping analysis of HT-siloxene electrode after cyclic test (Figure S15 (C-H)) indicates the presence of Si, O, C, N, B and F atoms distributed throughout the surface of the HT-siloxene electrode. The presence of C, N, B and F elements at the HT-siloxene electrode arises as a result of $EMIMBF_4$ electrolyte ions intercalation/de-intercalation process over prolong CD cycles. Figure S16 (A) shows the XPS survey spectrum of HT-siloxene electrode after cyclic test which revealed the presence of B 1s, C 1s, N 1s, and F 1s states in addition to the Si 2p and O 1s of the HT-siloxene. The core level spectrum of Si 2p state (Figure S16 (B)) observed at the binding energy of 101.7 eV was in consistent with the prepared HT-siloxene sheets. The core level spectrum of O 1s state shows the presence of oxygen in the interconnected Si rings of the HT-siloxene sheets[33,38]. Figure S16 (D-G) shows the core-level spectrum of C 1s, N 1s, B 1s, and

F 1s states which arises from the $EMIMBF_4$ electrolyte used in the HT-siloxene SSC. The binding energy values and spectral features of C 1s, N 1s, B 1s, and F 1s states are well matched with the XPS spectrum of $EMIMBF_4$ electrolyte.[56,57] In spite of having high energy storage capability and long cycle life of the fabricated HT-siloxene SSC, we examined for their use in practical applications. Initially, the HT-siloxene SSC was fully charged upto 3.0 V using a constant current of 0.5 mA, the stored energy in the HT-siloxene SSC can be utilized to power up electronic appliances. The fully charged HT-siloxene SSC is capable of glowing 10 commercial green LED for 15 s, 12 commercial blue LEDs for 25 s and a commercial blue night lamp for 10 s (inset of Figure. 6 (D)). These practical applications prove the proof of concept for the high-performance HT-siloxene SSC as a promising potency for future generation energy storage sectors.

Conclusion

We have demonstrated the removal of functional groups attached at the edges and basal planes of p-siloxene sheets via thermal annealing process. The chemical and structural analysis of as-prepared HT-siloxene sheets revealed that they are composed of oxygen enriched Si_6 rings with amorphous sheet-like structures. The investigation of HT-siloxene sheets as an electrode for supercapacitors demonstrated the high energy density of 15.53 mJ cm^{-2} (almost 2-fold higher compared to p-siloxene SSC) without compensating the power density. Further, HT-siloxene SSC possesses superior rate capability, low ESR value (compared to that of pristine-siloxene SSC) and better calendar life, thus demonstrating their excellent candidature towards the development of high-performance electrochemical energy storage devices. Future studies via advanced chemical/physical/thermal methods for complete removal of oxygenated functional groups bonded with siloxene sheets might result in the fundamental research development of chemically prepared silicenes and their practical application towards next-generation energy storage devices.

ASSOCIATED CONTENT

Supporting information

The electrochemical methods, supporting results and discussion, and comparative performance metrics of HT-siloxene SSC with the reported ones are provided in the electronic supporting information.

AUTHOR INFORMATION

Corresponding Author

*E-mail: kimsangj@jejunu.ac.kr (Prof. Sang -Jae Kim)

ORCID

Parthiban Pazhamalai: 0000-0003-0460-5763

Dr. Karthikeyan Krishnamoorthy: 0000-0002-8519-3010

Surjit Sahoo: 0000-0002-5378-1790

Vimal Kumar Mariappan: 0000-0002-7150-7920

Prof. Sang -Jae Kim: 0000-0002-5066-2622

Notes

"The authors declare no competing financial interest."

ACKNOWLEDGMENT

This research was supported by the Basic Science Research Program through the National Research Foundation of Korea (NRF) grant funded by the Korea government (MSIT) (2017R1C1B2012784 & 2018R1A4A1025998).

References:

(1) Kumar, K. S.; Choudhary, N.; Jung, Y.; Thomas, J. Recent Advances in Two-Dimensional Nanomaterials for Supercapacitor Electrode Applications. *ACS Energy Lett.* **2018**, *3* (2), 482–495.

(2) Acerce, M.; Voiry, D.; Chhowalla, M. Metallic 1T Phase MoS2 Nanosheets as Supercapacitor Electrode Materials. *Nat. Nanotechnol.* **2015**, *10* (4), 313–318.

(3) Kurra, N.; Ahmed, B.; Gogotsi, Y.; Alshareef, H. N. MXene-on-Paper Coplanar Microsupercapacitors. *Adv. Energy Mater.* **2016**, *6* (24), 1601372.

(4) Krishnamoorthy, K.; Pazhamalai, P.; Sahoo, S.; Kim, S.-J. Titanium Carbide Sheet Based High Performance Wire Type Solid State Supercapacitors. *J. Mater. Chem. A* **2017**, *5* (12), 5726–5736.

(5) Xu, G.; Nie, P.; Dou, H.; Ding, B.; Li, L.; Zhang, X. Exploring Metal Organic Frameworks for Energy Storage in Batteries and Supercapacitors. *Mater. Today* **2017**, *20* (4), 191–209.

(6) Liu, W.; Ulaganathan, M.; Abdelwahab, I.; Luo, X.; Chen, Z.; Rong Tan, S. J.; Wang, X.; Liu, Y.; Geng, D.; Bao, Y.; Chen, J.; Loh, K. P. Two-Dimensional Polymer Synthesized via Solid-State Polymerization for High-Performance Supercapacitors. *ACS Nano* **2018**, *12* (1), 852–860.

(7) Krishnamoorthy, K.; Pazhamalai, P.; Kim, S. J. Ruthenium Sulfide Nanoparticles as a New Pseudocapacitive Material for Supercapacitor. *Electrochim. Acta* **2017**, *227*, 85–94.

(8) Krishnamoorthy, K.; Pazhamalai, P.; Sahoo, S.; Lim, J. H.; Choi, K. H.; Kim, S. J. A High-Energy Aqueous Sodium-Ion Capacitor with Nickel Hexacyanoferrate and Graphene Electrodes. *ChemElectroChem* **2017**, *4* (12), 3302–3308.

(9) Chen, X.; Chen, K.; Wang, H.; Xue, D. Functionality of Fe(NO3)3 Salts as Both Positive

and Negative Pseudocapacitor Electrodes in Alkaline Aqueous Electrolyte. *Electrochim. Acta* **2014**, *147*, 216–224.

(10) Pazhamalai, P.; Krishnamoorthy, K.; Mariappan, V. K.; Sahoo, S.; Manoharan, S.; Kim, S.-J. A High Efficacy Self-Charging MoSe 2 Solid-State Supercapacitor Using Electrospun Nanofibrous Piezoelectric Separator with Ionogel Electrolyte. *Adv. Mater. Interfaces* **2018**, *5* (12), 1800055.

(11) Xue, Q.; Gan, H.; Huang, Y.; Zhu, M.; Pei, Z.; Li, H.; Deng, S.; Liu, F.; Zhi, C. Boron Element Nanowires Electrode for Supercapacitors. *Adv. Energy Mater.* **2018**, *8* (20), 1703117.

(12) Im, H. S.; Lim, Y. R.; Cho, Y. J.; Park, J.; Cha, E. H.; Kang, H. S. Germanium and Tin Selenide Nanocrystals for High-Capacity Lithium Ion Batteries: Comparative Phase Conversion of Germanium and Tin. *J. Phys. Chem. C* **2014**, *118* (38), 21884–21888.

(13) Chen, X.; Xu, G.; Ren, X.; Li, Z.; Qi, X.; Huang, K.; Zhang, H.; Huang, Z.; Zhong, J. A Black/Red Phosphorus Hybrid as an Electrode Material for High-Performance Li-Ion Batteries and Supercapacitors. *J. Mater. Chem. A* **2017**, *5* (14), 6581–6588.

(14) Ortaboy, S.; Alper, J. P.; Rossi, F.; Bertoni, G.; Salviati, G.; Carraro, C.; Maboudian, R. MnO x -Decorated Carbonized Porous Silicon Nanowire Electrodes for High Performance Supercapacitors. *Energy Environ. Sci.* **2017**, *10* (6), 1505–1516.

(15) Aradilla, D.; Gaboriau, D.; Bidan, G. G.; Gentile, P.; Boniface, M.; Dubal, D.; Gómez-Romero, P.; Wimberg, J.; Schubert, T. J. S.; Sadki, S. An Innovative 3-D Nanoforest Heterostructure Made of Polypyrrole Coated Silicon Nanotrees for New High Performance Hybrid Micro-Supercapacitors. *J. Mater. Chem. A* **2015**, *3* (26), 13978–13985.

(16) Zamfir, M. R.; Nguyen, H. T.; Moyen, E.; Lee, Y. H.; Pribat, D. Silicon Nanowires for Li-

Based Battery Anodes: A Review. *J. Mater. Chem. A* **2013**, *1* (34), 9566.

(17) Cui, Y. Functional Nanoscale Electronic Devices Assembled Using Silicon Nanowire Building Blocks. *Science (80-.).* **2001**, *291* (5505), 851–853.

(18) Xu, R.; Wang, G.; Zhou, T.; Zhang, Q.; Cong, H.-P.; Sen Xin; Rao, J.; Zhang, C.; Liu, Y.; Guo, Z.; Yu, S. H. Rational Design of Si@carbon with Robust Hierarchically Porous Custard-Apple-like Structure to Boost Lithium Storage. *Nano Energy* **2017**, *39*, 253–261.

(19) Zhao, J.; Liu, H.; Yu, Z.; Quhe, R.; Zhou, S.; Wang, Y.; Liu, C. C.; Zhong, H.; Han, N.; Lu, J.; Yao, Y.; Wu, K. Rise of Silicene: A Competitive 2D Material. *Prog. Mater. Sci.* **2016**, *83*, 24–151.

(20) Xue, D.; Sun, C.; Chen, X. Hybridization: A Chemical Bonding Nature of Atoms. *Chinese J. Chem.* **2017**, *35* (9), 1452–1458.

(21) Tchalala, M. R.; Ali, M. A.; Enriquez, H.; Kara, A.; Lachgar, A.; Yagoubi, S.; Foy, E.; Vega, E.; Bendounan, A.; Silly, M. G.; Sirotti, F.; Nitshe, S.; Chaudanson, D.; Jamgotchian, H.; Aufray, B.; Mayne, A. J.; Dujardin, G.; Oughaddou, H. Silicon Sheets by Redox Assisted Chemical Exfoliation. *J. Phys. Condens. Matter* **2013**, *25* (44), 442001.

(22) Galashev, A. Y.; Vorob'ev, A. S. Physical Properties of Silicene Electrodes for Li-, Na-, Mg-, and K-Ion Batteries. *J. Solid State Electrochem.* **2018**, *22* (11), 3383–3391.

(23) Tokmachev, A. M.; Averyanov, D. V.; Parfenov, O. E.; Taldenkov, A. N.; Karateev, I. A.; Sokolov, I. S.; Kondratev, O. A.; Storchak, V. G. Emerging Two-Dimensional Ferromagnetism in Silicene Materials. *Nat. Commun.* **2018**, *9* (1), 1672.

(24) Lv, J.; Xu, M.; Lin, S.; Shao, X.; Zhang, X.; Liu, Y.; Wang, Y.; Chen, Z.; Ma, Y. Direct-Gap Semiconducting Tri-Layer Silicene with 29% Photovoltaic Efficiency. *Nano Energy* **2018**, *51*, 489–495.

(25) Wei, W.; Dai, Y.; Huang, B. Hydrogenation of Silicene on Ag(111) and Formation of Half-Silicane. *J. Mater. Chem. A* **2017**, *5* (34), 18128–18137.

(26) Satta, M.; Lacovig, P.; Apostol, N.; Dalmiglio, M.; Orlando, F.; Bignardi, L.; Bana, H.; Travaglia, E.; Baraldi, A.; Lizzit, S.; Larciprete, R. The Adsorption of Silicon on an Iridium Surface Ruling out Silicene Growth. *Nanoscale* **2018**, *10* (15), 7085–7094.

(27) Shoji Yamanaka, Hiroyuki Matsu-ura, M. I. New Deintercalation Reaction of Calcium from Calcium Disilicide. Synthesis of Layered Polysilane. *Mater. Res. Bull.* **1996**, *31* (3), 307–316.

(28) Liu, J.; Yang, Y.; Lyu, P.; Nachtigall, P.; Xu, Y. Few-Layer Silicene Nanosheets with Superior Lithium-Storage Properties. *Adv. Mater.* **2018**, *30* (26), 1800838.

(29) Zhang, X.; Qiu, X.; Kong, D.; Zhou, L.; Li, Z.; Li, X.; Zhi, L. Silicene Flowers: A Dual Stabilized Silicon Building Block for High-Performance Lithium Battery Anodes. *ACS Nano* **2017**, *11* (7), 7476–7484.

(30) Zhang, W.; Sun, L.; Nsanzimana, J. M. V.; Wang, X. Lithiation/Delithiation Synthesis of Few Layer Silicene Nanosheets for Rechargeable Li-O 2 Batteries. *Adv. Mater.* **2018**, *30* (15), 1705523.

(31) Imagawa, H.; Itahara, H. Stabilized Lithium-Ion Battery Anode Performance by Calcium-Bridging of Two Dimensional Siloxene Layers. *Dalt. Trans.* **2017**, *46* (11), 3655–3660.

(32) Fu, R.; Zhang, K.; Zaccaria, R. P.; Huang, H.; Xia, Y.; Liu, Z. Two-Dimensional Silicon Suboxides Nanostructures with Si Nanodomains Confined in Amorphous SiO 2 Derived from Siloxene as High Performance Anode for Li-Ion Batteries. *Nano Energy* **2017**, *39* (July), 546–553.

(33) Krishnamoorthy, K.; Pazhamalai, P.; Kim, S.-J. Two-Dimensional Siloxene Nanosheets:

Novel High-Performance Supercapacitor Electrode Materials. *Energy Environ. Sci.* **2018**, *11* (6), 1595–1602.

(34) Dahn, J. R.; Way, B. M.; Fuller, E.; Tse, J. S. Structure of Siloxene and Layered Polysilane (Si6H6). *Phys. Rev. B* **1993**, *48* (24), 17872–17877.

(35) Li, S.; Wang, H.; Li, D.; Zhang, X.; Wang, Y.; Xie, J.; Wang, J.; Tian, Y.; Ni, W.; Xie, Y. Siloxene Nanosheets: A Metal-Free Semiconductor for Water Splitting. *J. Mater. Chem. A* **2016**, *4* (41), 15841–15844.

(36) Nakano, H.; Ishii, M.; Nakamura, H. Preparation and Structure of Novel Siloxene Nanosheets. *Chem. Commun.* **2005**, *2* (23), 2945.

(37) Yamanaka, S.; Matsu-ura, H.; Ishikawa, M.; Shoji Yamanaka, Hiroyuki Matsu-ura, M. I. New Deintercalation Reaction of Calcium from Calcium Disilicide. Synthesis of Layered Polysilane. *Mater. Res. Bull.* **1996**, *31* (3), 307–316.

(38) Dahn, J. R.; Way, B. M.; Fuller, E. W.; Weydanz, W. J.; Tse, J. S.; Klug, D. D.; Van Buuren, T.; Tiedje, T. X-ray Diffraction and X-ray Absorption Studies of Porous Silicon, Siloxene, Heat-treated Siloxene, and Layered Polysilane. *J. Appl. Phys.* **1994**, *75* (4), 1946–1951.

(39) Ubara, H.; Imura, T.; Hiraki, A.; Hirabayashi, I.; Morigaki, K. Structural Change from Crystalline to Amorphous States in Siloxene by Thermal Annealing. *J. Non. Cryst. Solids* **1983**, *59–60*, 641–644.

(40) Stankovich, S.; Dikin, D. A.; Piner, R. D.; Kohlhaas, K. A.; Kleinhammes, A.; Jia, Y.; Wu, Y.; Nguyen, S. T.; Ruoff, R. S. Synthesis of Graphene-Based Nanosheets via Chemical Reduction of Exfoliated Graphite Oxide. *Carbon N. Y.* **2007**, *45* (7), 1558–1565.

(41) Imagawa, H.; Takahashi, N.; Nonaka, T.; Kato, Y.; Nishikawa, K.; Itahara, H. Synthesis of a Calcium-Bridged Siloxene by a Solid State Reaction for Optical and Electrochemical

Properties. *J. Mater. Chem. A* **2015**, *3* (18), 9411–9414.

(42) Yan, R.; Antonietti, M.; Oschatz, M. Toward the Experimental Understanding of the Energy Storage Mechanism and Ion Dynamics in Ionic Liquid Based Supercapacitors. *Adv. Energy Mater.* **2018**, *8* (18), 1800026.

(43) Shpigel, N.; Lukatskaya, M. R.; Sigalov, S.; Ren, C. E.; Nayak, P.; Levi, M. D.; Daikhin, L.; Aurbach, D.; Gogotsi, Y. In Situ Monitoring of Gravimetric and Viscoelastic Changes in 2D Intercalation Electrodes. *ACS Energy Lett.* **2017**, *2* (6), 1407–1415.

(44) Zhang, S.; Pan, N. Supercapacitors Performance Evaluation. *Adv. Energy Mater.* **2015**, *5* (6), 1401401.

(45) Aradilla, D.; Gentile, P.; Bidan, G.; Ruiz, V.; Gómez-Romero, P.; Schubert, T. J. S.; Sahin, H.; Frackowiak, E.; Sadki, S. High Performance of Symmetric Micro-Supercapacitors Based on Silicon Nanowires Using N-Methyl-N-Propylpyrrolidinium Bis(Trifluoromethylsulfonyl)Imide as Electrolyte. *Nano Energy* **2014**, *9*, 273–281.

(46) Aradilla, D.; Gao, F.; Lewes-Malandrakis, G.; Müller-Sebert, W.; Gentile, P.; Pouget, S.; Nebel, C. E.; Bidan, G. Powering Electrodes for High Performance Aqueous Micro-Supercapacitors: Diamond-Coated Silicon Nanowires Operating at a Wide Cell Voltage of 3 V. *Electrochim. Acta* **2017**, *242*, 173–179.

(47) Aradilla, D.; Bidan, G.; Gentile, P.; Weathers, P.; Thissandier, F.; Ruiz, V.; Gómez-Romero, P.; Schubert, T. J. S.; Sahin, H.; Sadki, S. Novel Hybrid Micro-Supercapacitor Based on Conducting Polymer Coated Silicon Nanowires for Electrochemical Energy Storage. *RSC Adv.* **2014**, *4* (50), 26462.

(48) Chatterjee, S.; Carter, R.; Oakes, L.; Erwin, W. R.; Bardhan, R.; Pint, C. L. Electrochemical and Corrosion Stability of Nanostructured Silicon by Graphene Coatings: Toward High

Power Porous Silicon Supercapacitors. *J. Phys. Chem. C* **2014**, *118* (20), 10893–10902.

(49) Aradilla, D.; Gao, F.; Lewes-Malandrakis, G.; Müller-Sebert, W.; Gaboriau, D.; Gentile, P.; Iliev, B.; Schubert, T.; Sadki, S.; Bidan, G.; Nebel, C. E. A Step Forward into Hierarchically Nanostructured Materials for High Performance Micro-Supercapacitors: Diamond-Coated SiNW Electrodes in Protic Ionic Liquid Electrolyte. *Electrochem. commun.* **2016**, *63*, 34–38.

(50) El-Kady, M. F.; Kaner, R. B. Scalable Fabrication of High-Power Graphene Micro-Supercapacitors for Flexible and on-Chip Energy Storage. *Nat. Commun.* **2013**, *4* (1), 1475.

(51) Krishnamoorthy, K.; Pazhamalai, P.; Veerasubramani, G. K.; Kim, S. J. Mechanically Delaminated Few Layered MoS 2 Nanosheets Based High Performance Wire Type Solid-State Symmetric Supercapacitors. *J. Power Sources* **2016**, *321*, 112–119.

(52) Choi, C.; Kim, K. M.; Kim, K. J.; Lepró, X.; Spinks, G. M.; Baughman, R. H.; Kim, S. J. Improvement of System Capacitance via Weavable Superelastic Biscrolled Yarn Supercapacitors. *Nat. Commun.* **2016**, *7*, 13811.

(53) Gaboriau, D.; Aradilla, D.; Brachet, M.; Le Bideau, J.; Brousse, T.; Bidan, G.; Gentile, P.; Sadki, S. Silicon Nanowires and Nanotrees : Elaboration and Optimization of New 3D Architectures for High Performance on-Chip Supercapacitors. *soumis à Nano Energy* **2015**, *6*, 81017–81027.

(54) Thissandier, F.; Pauc, N.; Brousse, T.; Gentile, P.; Sadki, S. Micro-Ultracapacitors with Highly Doped Silicon Nanowires Electrodes. *Nanoscale Res. Lett.* **2013**, *8* (1), 38.

(55) Xia, X.; Tu, J.; Zhang, Y.; Wang, X.; Gu, C.; Zhao, X.-B.; Fan, H. J. High-Quality Metal Oxide Core/Shell Nanowire Arrays on Conductive Substrates for Electrochemical Energy Storage. *ACS Nano* **2012**, *6* (6), 5531–5538.

(56) Blundell, R. K.; Licence, P. Quaternary Ammonium and Phosphonium Based Ionic Liquids: A Comparison of Common Anions. *Phys. Chem. Chem. Phys.* **2014**, *16* (29), 15278–15288.

(57) Tõnisoo, A.; Kruusma, J.; Pärna, R.; Kikas, A.; Hirsimäki, M.; Nõmmiste, E.; Lust, E. In Situ XPS Studies of Electrochemically Negatively Polarized Molybdenum Carbide Derived Carbon Double Layer Capacitor Electrode. *J. Electrochem. Soc.* **2013**, *160* (8), A1084–A1093.

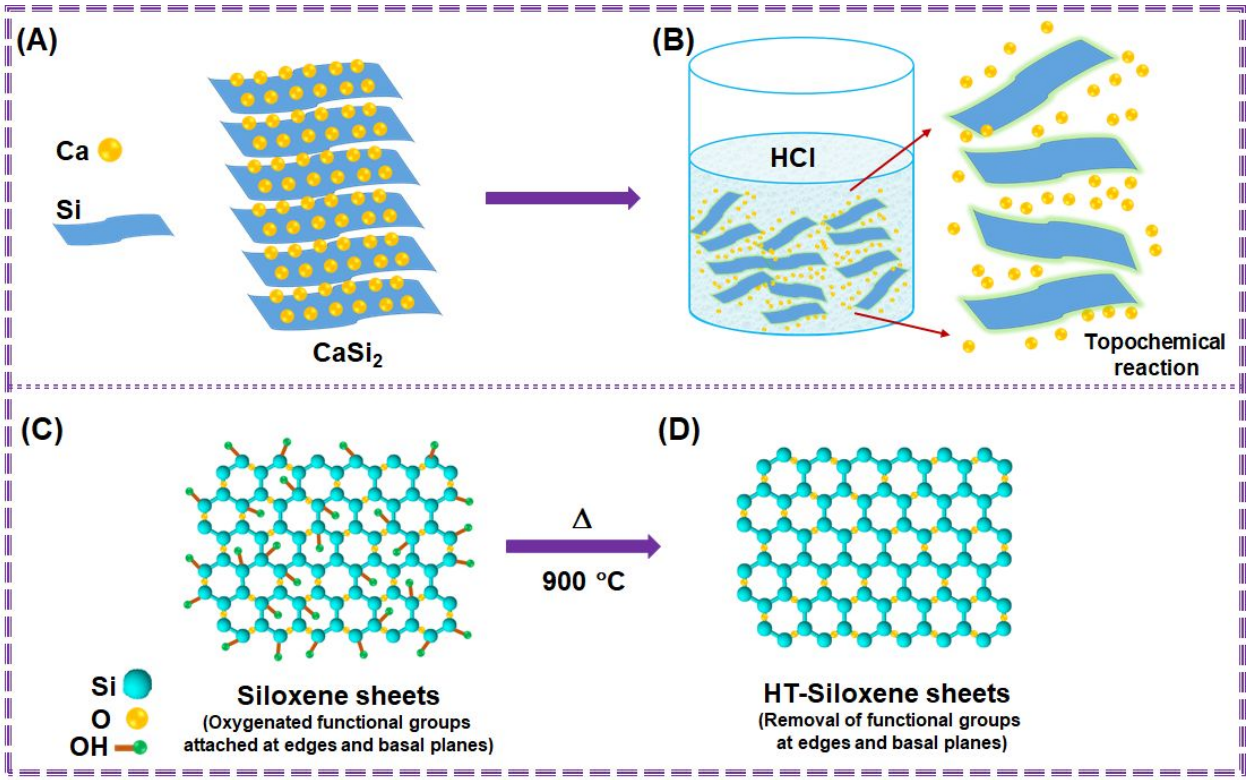

Figure 1. Schematic representation of the preparation of HT-siloxene sheets. (A-B) Preparation of p-siloxene sheets from $CaSi_2$ via a topochemical reaction, (C) structure of the resulting p-siloxene sheets with oxygenated functional groups. (D) structure of the HT-siloxene sheets after heat treatment of 900 ºC.

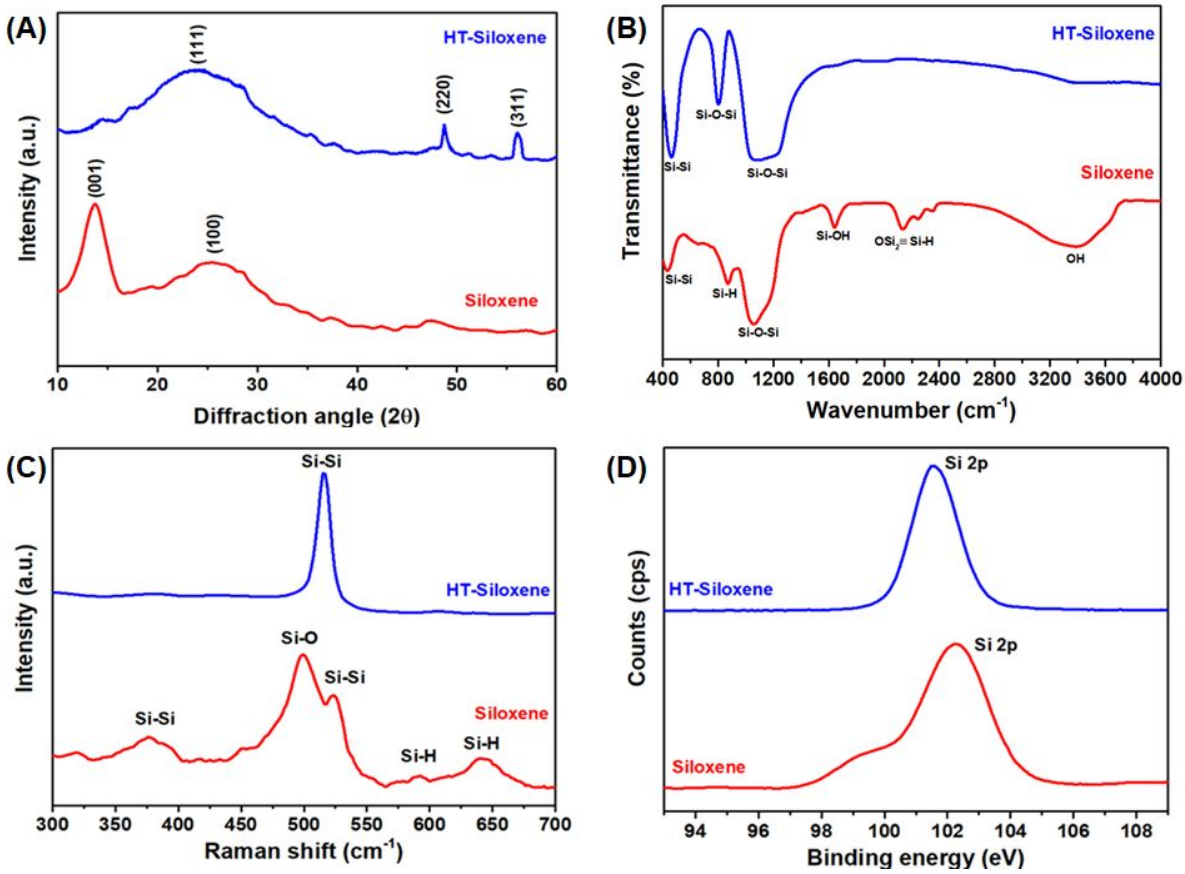

Figure 2. Physicochemical characterization of p-siloxene and HT-siloxene sheets. (A) X-ray diffraction pattern of the p-siloxene and HT-siloxene sheets. (B) Fourier transform infrared spectrum of p-siloxene and HT-siloxene sheets. (C) Laser Raman spectra of the p-siloxene and HT-siloxene sheets. X-ray photoelectron spectroscopy of the p-siloxene and HT-siloxene sheets (D) Core-level X-ray photoelectron spectra for Si 2p states of p-siloxene and HT-siloxene sheets.

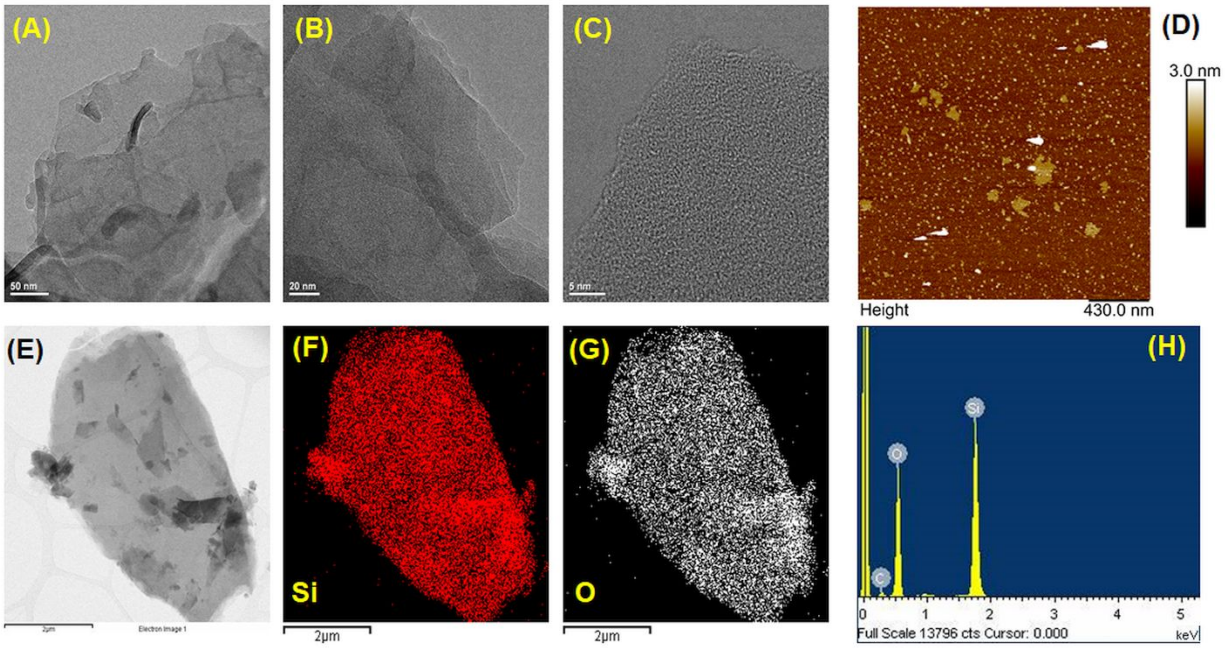

Figure 3. (A-C) High-resolution transmission electron microscopy (HR-TEM) images, (D) tapping-mode atomic force micrograph of the HT-siloxene sheets, (E-H) overlay image, elemental mapping of Si atoms and oxygen atoms with corresponding EDS mapping table of the HT-siloxene sheets.

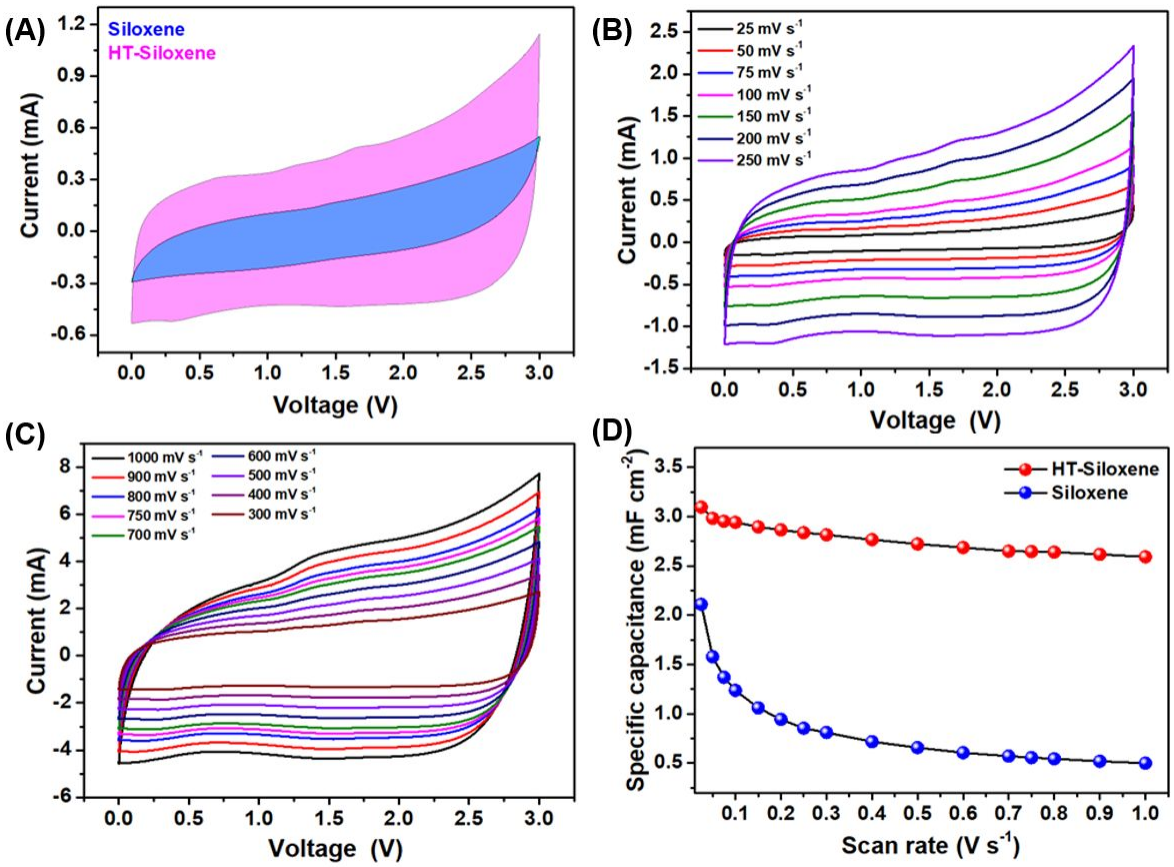

Figure 4. Electrochemical analysis of the p-siloxene and HT-siloxene-based symmetric supercapacitor (SSC) device (CR2032 coin cell) in 1-Ethyl-3-methylimidazolium tetrafluoroborate ($EMIMBF_4$). (A) Cyclic voltammetric profile of the p-siloxene and HT-siloxene SSCs measured over operating voltage window from 0.0 to 3.0 V using a scan rate of 100 mV s^{-1}. (B-C) Cyclic voltammetric profiles of HT-siloxene SSCs measured using different scan rates from 25 to 1000 mV s^{-1}. (D) Variation of areal specific capacitance of p- siloxene and HT-siloxene SSCs with respect to scan rate.

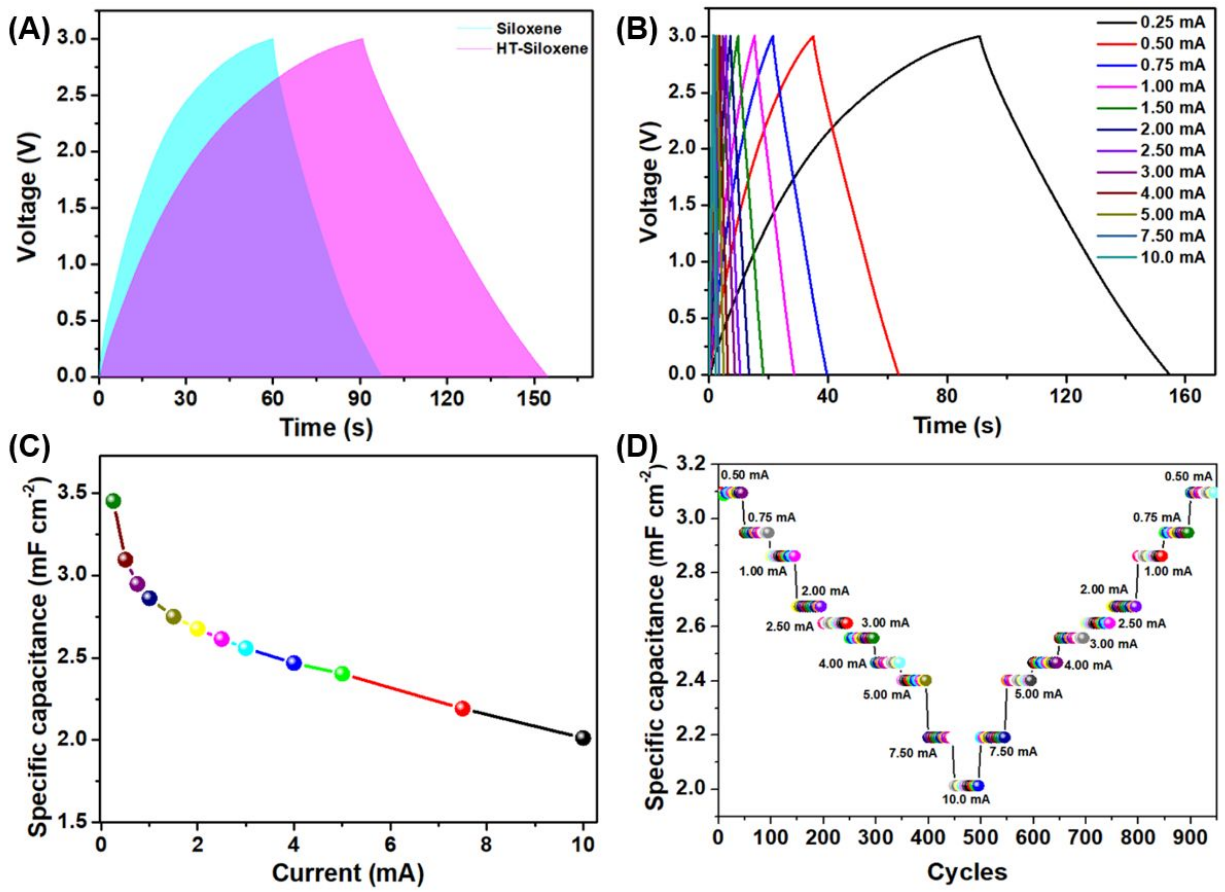

Figure 5. (A) Galvanostatic charge–discharge profile of the p-siloxene and HT-siloxene SSCs measured using a constant current of 0.25 mA. (B) Charge–discharge profiles of HT-siloxene SSC obtained using various applied current ranges. (C) Effect of discharge current on the specific capacitance of the siloxene and HT-siloxene SSCs ensuring the enhanced electrochemical properties of HT-siloxene. (D) Rate capability studies of the HT-siloxene SSC.

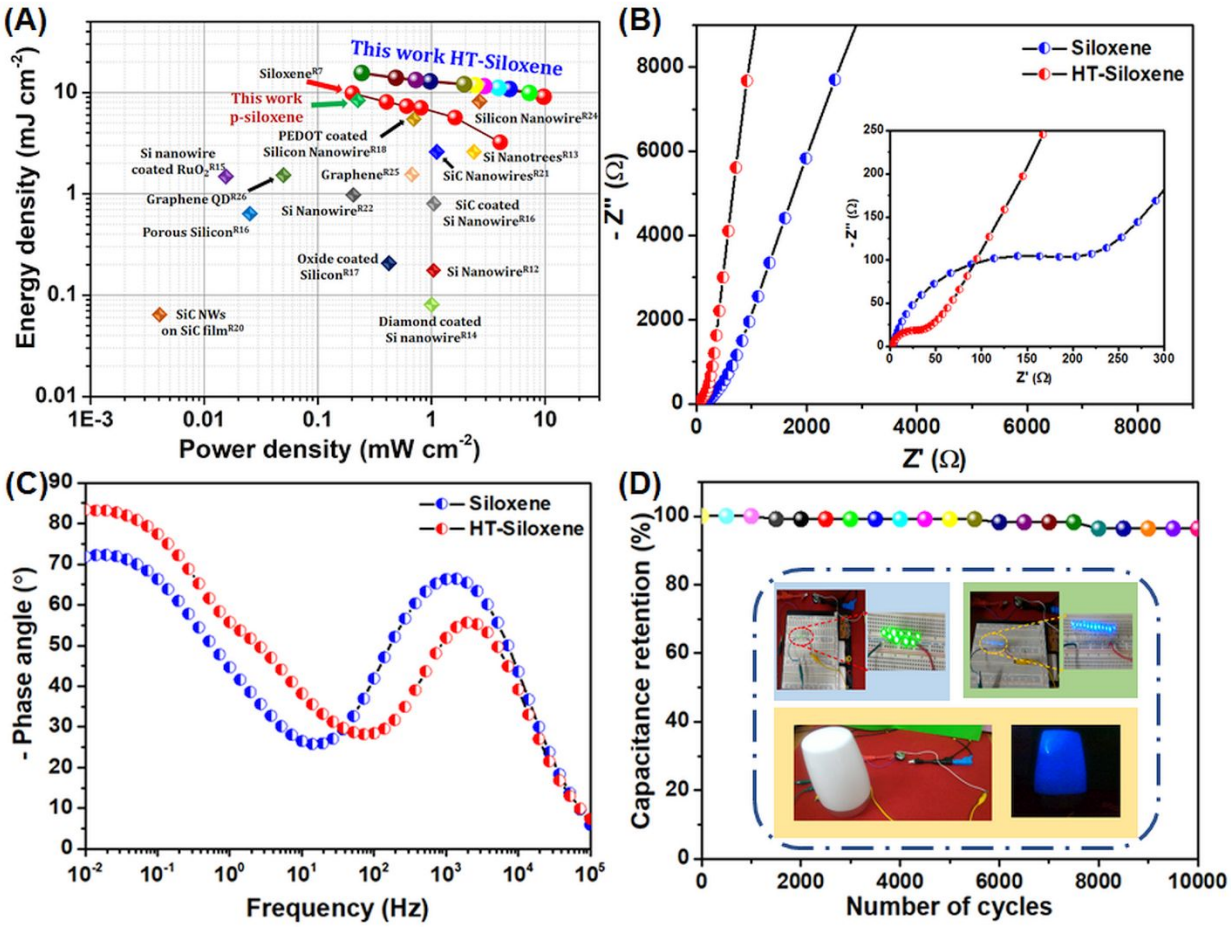

Figure 6. (A) Ragone plot of the HT-siloxene SSC showing the superior performance metrics over the reported Si-based SSCs (The electrolyte, OPW, specific capacitance, energy/power density of the references given in Figure 6(A) were provided in the Table S1, SI). The Electrochemical impedance spectroscopic analysis of the p-siloxene and HT-siloxene SSCs analyzed using (B) Nyquist plot and (C) Bode phase angle plot. (D) Cycling stability of the HT-siloxene SSC over 10,000 continuous charge–discharge cycles. The inset in (D) shows the practical application of fully charged HT-siloxene SSC to glow (i) 10 commercial green LEDs; (ii) glow 12 commercial blue LEDs and (iii) powering a blue LED based night lamp.

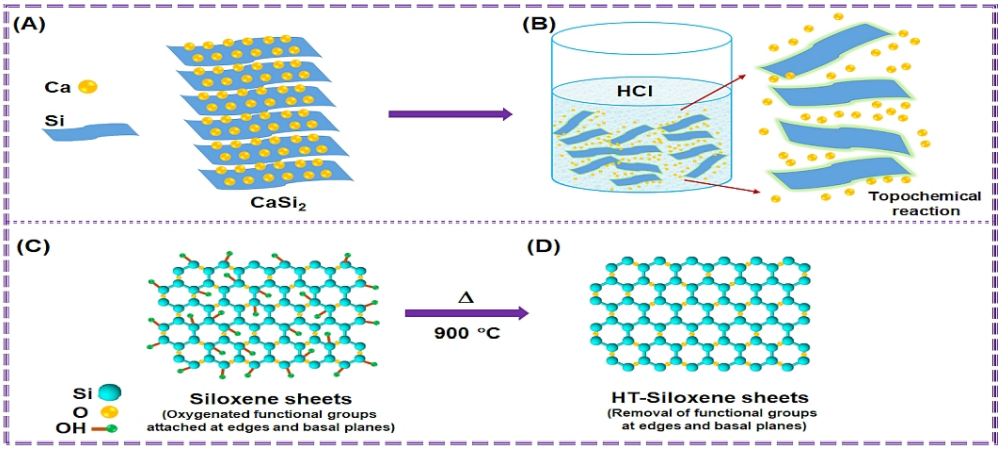

90x39mm (300 x 300 DPI)